

Design Optimization of Directly Grid-Connected PM Machines for Wind Energy Applications

Johannes H. J. Potgieter, *Member, IEEE*, and Maarten J. Kamper, *Senior Member, IEEE*

Abstract—The focus of the study in this paper is on the design of unconventional directly grid-connected PM wind generators without power electronic converters. As a case study, this analysis is based on a novel direct-drive wind generator system known as a slip-synchronous permanent-magnet (PM) wind generator. Attention is given to the definition of the design requirements of the directly grid-connected synchronous-generator unit from the relevant grid code specifications and to find the optimum design subject to these requirements. Due to the direct-grid connection, there are clear differences in the design requirements of this machine and those of conventional PM wind generators connected to the grid via a converter. Four different generator topologies are evaluated with regard to the ease of manufacturing, active mass, PM content, and suitability for direct-grid connection. Both simulated and measured results are given for an experimental direct-grid slip-synchronous PM generator.

Index Terms—Permanent-magnet (PM) machines, power grids, wind energy generation, wind energy integration.

NOMENCLATURE

D_i	Generator inside diameter, mm.
D_o	Maximum outer diameter, mm.
l	Axial length of generator, mm.
M_{Cu}	Conductor mass, kg.
M_{Fe}	Electrical steel mass, kg.
M_{PM}	Permanent magnet (PM) mass, kg.
M_{Tot}	Total active mass, kg.
n_s	Rated turbine speed, r/min.
T_b	Maximum breakdown torque, p.u.
T_s	Developed generator torque, N · m.
v_{min}	Cut-in wind speed, m/s.
v_w	Rated wind speed, m/s.
I_d	Steady-state d -axis current, A.
I_q	Steady-state q -axis current, A.
I_{rms}	RMS grid line current, A.
V_{rms}	RMS grid voltage per phase, V.

L_d	d -axis inductance, H.
L_q	q -axis inductance, H.
L_e	End-winding inductance, H.
L_s	Per-phase synchronous inductance, H.
p	Number of PM-rotor poles.
P_{cu}	Stator winding conductor losses, W.
P_{ecr}	Stator core losses, W.
P_{ecs}	PM-rotor core and PM eddy-current losses, W.
P_{wf}	Wind and friction losses, W.
P_s	Generator active power, kW.
Q_s	Generator reactive power, kW.
R_b	Braking resistance load, Ω .
R_s	Resistance per phase, Ω .
V_d	Steady-state d -axis voltage, V.
V_q	Steady-state q -axis voltage, V.
X_s	Synchronous impedance, Ω .
X	Dimensional input parameters.
Y	Performance output parameters.
α_s	Current angle, $^\circ$.
Δ	Load angle, $^\circ$.
$\Delta\tau_L$	Rated load torque ripple, %.
$\Delta\tau_{NL}$	No-load cogging torque, %.
η_r	Slip permanent-magnet generator (slip-PMG) unit efficiency, %.
η_s	Permanent-magnet synchronous generator (PMSG) unit efficiency, %.
η_t	Total generator system efficiency, %.
λ_d	d -axis flux linkage, Wb.t.
λ_q	q -axis flux linkage, Wb.t.
λ_m	PM flux linkage, Wb.t.
θ	Power factor (PF) angle, $^\circ$.
ω_b	Maximum breakdown torque speed value, rad/s.
ω_s	Synchronous grid speed, rad/s.

I. INTRODUCTION

Manuscript received December 6, 2014; accepted December 17, 2014. Date of publication January 22, 2015; date of current version July 15, 2015. Paper 2014-EMC-0601, presented at the 2013 IEEE Energy Conversion Congress and Exposition, Denver, CO, USA, September 16–20, and approved for publication in the IEEE TRANSACTIONS ON INDUSTRY APPLICATIONS by the Electric Machines Committee of the IEEE Industry Applications Society. This work was supported in part by the National Research Foundation and in part by the Technology Innovation Agency of South Africa.

J. H. J. Potgieter is with the Department of Engineering Science, University of Oxford, Oxford, OX1 3PJ, U.K. (e-mail: johannes.potgieter@eng.ox.ac.uk).

M. J. Kamper is with the Department of Electrical and Electronic Engineering, Stellenbosch University, Stellenbosch 7599, South Africa (e-mail: kamper@sun.ac.za).

Color versions of one or more of the figures in this paper are available online at <http://ieeexplore.ieee.org>.

Digital Object Identifier 10.1109/TIA.2015.2394506

WITH the penetration levels of wind energy and other types of renewable energy increasing at an ever growing pace, several issues are arising which need to be addressed. Obvious issues are the reduction of the initial capital cost of these installations and increasing the energy yield. However, other aspects growing in importance are the improvement of the grid compliance of wind generator systems and increased reliability. Important grid connection aspects of wind generators relate to the behavior of the wind turbine during grid faults, reactive power characteristics, and grid inertial support. Reliability is important to reduce the operation and maintenance (O&M) costs of these systems. O&M is especially important

for systems with limited access, such as offshore turbines where it is essential that O&M are reduced to a minimum.

In [1], a summary is given of the current trends of wind generator technologies as well as the disadvantages of each. At present, most installed systems make use of a doubly fed induction generator (DFIG), with a gearbox and a partially rated power electronic converter. Due to gearbox failures owing to high financial implications, direct-drive gearless PM generators connected to the grid via a full rated power electronic converter are considered in many new installations. However, due to the current high cost of PM material, synchronous generators (SGs) with wound rotors and smaller medium-speed PM generators operated with a lower gearing ratio gearbox, which are considered more reliable, are considered as well. Some manufacturers also utilize the conventional squirrel-cage induction machine and full rated power electronic converter due to the low system cost of these installations. Although not as severe as gearbox failures and with components easier to replace, electrical failures are the most common type of failure for wind generator systems. Thus, it is clear that, if the gearbox and power electronic converter are simplified or even removed from the drivetrain, the reliability of wind turbine systems can be increased significantly. Some further background on reliability and the failure rate of the different components in wind turbine systems can be found in [2] for small-scale systems and in [3] for utility-scale wind turbine systems.

The approach taken in this paper is to propose the use of a directly grid-connected wind generator topology to address some of these issues. The aim is to determine what the design approach would be for such a system and whether these systems are a feasible alternative to conventional technologies. Very few studies exist in this regard, and no clear indication can be found in the literature on the exact design requirements of these types of wind generators. The directly grid-connected wind turbine topology used as a case study in this paper is known as a slip-synchronous permanent-magnet wind generator (SS-PMG) as introduced in [4]. The focus is on the design of the directly grid-connected synchronous wind generator part of the generator system. Optimum finite element (FE) designs are given for four different PM generator topologies. The suitability of the different topologies for direct-grid connection are also evaluated. Aspects generally considered in PM wind generator design such as active mass, PM content, ease of manufacturing, load, and especially no-load cogging torque characteristics are taken into account as well. Due to practical considerations, a 15-kW directly grid-connected SS-PMG wind turbine system is used as a case study. Measurements taken in both the laboratory and in the field for an installed 15-kW wind turbine system are presented as well.

II. DIRECT-GRID WIND GENERATOR TECHNOLOGIES

Although not extensively used in wind energy systems, directly grid-connected SGs have been successfully used for decades for conventional power generation with widespread acceptance by both the power generation industry and network operators.

While limited and with most only conceptual, there are other studies in the literature on directly grid-connected PM syn-

chronous wind generators. In many conventional SGs, damper windings are used, but these are not deemed adequate for wind generator applications. However, there are some studies in the literature where external damping systems are proposed for direct-grid synchronous wind generators. In [5], a spring and damper system is used to damp the power angle oscillations of a directly grid-connected PMSG. Another example is the concept as proposed in [6] where a partially rated converter is placed in the star point of the generator to damp oscillations resulting from load variations.

Several studies are currently being conducted on devices where the variable-speed input from the turbine is transformed to a fixed-speed output at the generator side which enables the direct-grid connection of an SG. There are also certain studies where hard gearing with physical gear changes is proposed. Many of these systems, however, employ continuously-variable-transmission topologies. Some concepts allow a direct-grid connection by connecting the generator to the turbine via a hydraulic system. One example is the hydrodynamically controlled gearbox with a fixed-speed output and variable-speed input as discussed in [7]. This paper includes an in-depth study regarding the grid connection aspects of the directly grid-connected SG. Several favorable grid connection characteristics are mentioned. Studies based on hydrostatic hydraulic wind power transfer systems making use of positive displacement pumps are also gaining in momentum, as originally proposed by Salter and Rea [8] with a more recent example in [9].

Getting closer to the topology evaluated in this paper is a concept known as a permanent-magnet induction generator (PMIG). The concept was first introduced by Punga and Schon [10] in 1926. Initially, the PMIG was proposed to improve the PF of conventional induction machines, with later studies, as in [11] and [12], proposing it for use as a direct-drive directly grid-connected PM wind generator. In [13], a PMIG-type topology similar to a DFIG is proposed. By connecting a partially rated converter to the rotor terminals, the PMIG can be operated as a variable-speed wind generator. Several other studies exist on this concept, with the contribution of each of the relevant literature works thoroughly discussed in [4].

The SS-PMG that was recently introduced in [4] is based upon the PMIG concept, with the difference being that the stator and slip-rotor windings are electromagnetically separated. The SS-PMG consists of two integrated generating units, a slip-PMG which is fixed to the turbine, and a PMSG connected directly to the grid. These generating units are mechanically linked by a common PM rotor with separate sets of PMs for each. A cross-sectional diagram of an SS-PMG is shown in Fig. 1(a). A voltage is induced in the windings of the slip-PMG at slip frequency and in the PMSG at synchronous frequency as explained in the equivalent circuit of the SS-PMG in Fig. 1(b). The evaluation and optimum design of the slip-PMG unit is thoroughly covered in [14], and the work done in [15] focuses on the stability analysis of the SS-PMG. Thus, with the concept introduced in [16], the slip-PMG unit design covered in [14], and the stability of the direct-grid SS-PMG evaluated in [15], the focus of this paper is on the optimum design of the PMSG unit. This aspect has not been covered in detail in any of the previous publications before.

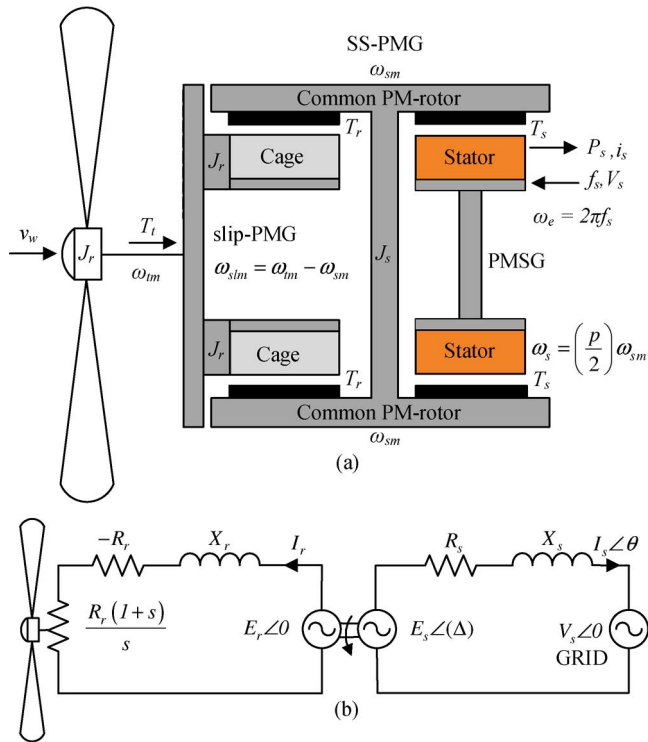


Fig. 1. (a) SS-PMG cross-sectional diagram and (b) equivalent circuit [4].

Apart from an expected improvement in reliability by simplifying or removing the gearbox and power electronic converter from the drivetrain, direct-drive SGs have several advantages. With higher penetration of wind power, a major concern is the loss of grid inertia, i.e., due to the rotor, which provides a significant spinning reserve, being decoupled from the grid due to the use of power electronic converters as discussed in [17]. By reducing the grid inertia, it becomes much more susceptible to sudden load variations, with a much lower inertial buffer to counteract against frequency variations. It is thus anticipated that future grid-code requirements would require the wind farm operator to contribute to the grid inertia. The direct-grid wind generator topologies might thus have some advantage in this regard. However, more work is still required to gain a better understanding on this aspect. As mentioned in [7], the directly grid-connected SG can more easily provide a higher amount of reactive power compensation with respect to other wind generator topologies currently in use. Based upon the system in [7], there are also certain applications at the distribution level where the directly grid-connected SG is implemented as a synchronous condenser to compensate for grid voltage variations.

III. DESIGN SPECIFICATIONS

The design requirements of the directly grid-connected SS-PMG are assessed in two parts in this section. First the relevant grid-code specifications are summarized, and second, the requirements for the specific turbine system and direct-drive wind generators in general are discussed. Furthermore, the whole aim of the SS-PMG is to have an as simple and robust as possible wind generator system. This design methodology is thus applied throughout the whole generator design process.

A. Direct-Grid Specifications

For this paper, the local applicable grid codes and regulations for wind turbine facilities are used as a basis to obtain the design specifications of the generator as stipulated in [18]. The SS-PMG is synchronized to the grid by means of a grid-synchronization controller as explained in [19]. For utility-scale systems, an electronically controlled tap-changing transformer configuration is proposed to monitor and change the terminal voltage at the point of common coupling (PCC) as required by the utility and as explained in [20]. In [21] and [15], the low voltage ride through (LVRT) capabilities of the SS-PMG are evaluated. The systems as mentioned earlier are responsible for the implementation of the grid-code requirements. However, it is still necessary that the generator design complies with many of the aspects listed hereinafter.

- 1) From a 0.2-p.u. generator load, the PF should not be less than 0.95 leading or lagging for systems < 1 MVA, 0.975 leading or lagging for systems > 1 MVA and < 20 MVA, and 0.95 leading or lagging for systems > 20 MVA.
- 2) For systems > 1 MVA, reactive power and voltage control are required at the PCC as specified by the utility and as in [18]. This is not a requirement for systems < 1 MVA.
- 3) Reactive power and voltage should be controlled with a tolerance of 0.5% of the rated power.
- 4) The system needs to be able to operate in a voltage range of $\pm 10\%$ around the nominal voltage for wind energy facilities > 100 kVA and between $+10\%$ and -15% for systems < 100 kVA at the PCC continuously.
- 5) The system should stay connected to the grid during low-voltage and overvoltage conditions as stipulated by the regimes shown in [18] and also evaluated in [15].
- 6) In some cases, active power control is needed, particularly during grid frequency variations, to reduce the power delivered to the grid.
- 7) Frequency variations between 47 and 52 Hz at a rate of change of 1.5 Hz/s need to be accommodated by the wind generator system.
- 8) The quality of the power delivered should comply to the limit set, as agreed to by the utility. An example is the specifications based on the IEC 61727:2004 standard as given in [22] for small-scale embedded generation. Individual current distortion limits are provided for the different harmonics, and a total harmonic distortion (THD) limit of 5% is given. The generator needs to comply to the limit set from 0.2-p.u. load.
- 9) It is also important that voltage fluctuations caused by flickering effects are reduced and monitored at the PCC at all times.

B. Design Issues in General

Several works on the design and comparison of direct-drive PM generators with regard to other drivetrain topologies are available in the literature as, for example, in [23] and [24]. The issues identified in the design and implementation of direct-drive PM wind generators are the high cost, with this generator type currently being the most expensive drivetrain solution in use, the high cost and also the volatility of PM prices, the high active mass and also the structural mass at higher power levels,

TABLE I
DESIGN CONSTRAINTS OF THE 15-kW CASE STUDY SS-PMG SYSTEM

Parameter	Value
Rated torque, $T_{s(rated)}$, Nm	1000
Maximum breakdown torque T_b , pu	≥ 2.0
No-load cogging torque, $\Delta\tau_{NL}$, %	≤ 2.5
Full-load torque ripple, $\Delta\tau_L$, %	≤ 4.0
Required rated efficiency, η_s , %	≥ 94
Maximum outer diameter, D_o , mm	655
Minimum wind speed, v_{min} , m/s	4
Rated wind speed, v_w , m/s	11
Rated rotor speed n_s , r/min	150
Grid line voltage $\sqrt{3}V_{rms}$, V	400
Grid frequency F_s , Hz	50

and the large size which makes assembly, installation, and transport difficult. It is thus essential that the mass and PM content of these generators be made as low as possible in the design optimization. Other aspects include the ease of manufacturing and segmentation, particularly for larger generators. Furthermore, what is important in the design of PM generators is the no-load cogging torque which hampers the start-up of the wind generator and also the stability. Methods to reduce the torque ripple are discussed in [25].

For the 15-kW case study system under consideration, Table I gives some of the constraints associated with this design. From the turbine curves for the 15-kW wind generator system to be implemented, a rated torque value of $T_{rated} = 1000 \text{ N} \cdot \text{m}$, at a rated turbine speed of $n_s = 150 \text{ r/min}$ and a rated wind speed of $v_w = 11 \text{ m/s}$, is selected. From the dimensions of the evaluated turbine, the maximum outer diameter of the generator is fixed at $D_o = 655 \text{ mm}$. Normally, for utility-scale systems making use of mechanical and aerodynamic braking, the maximum torque seldom exceeds a value of $T_b \geq 1.5 \text{ p.u.}$ However, for the 15-kW fixed-pitch system under consideration, electromagnetic braking is employed, and in this case, the maximum torque is specified as $T_b \geq 2.0 \text{ p.u.}$ [26]. From previous studies such as the design in [25], a no-load cogging torque value of $\Delta\tau_{NL} \leq 2.5\%$ and a load torque ripple of $\Delta\tau_L \leq 4\%$ are specified. In some cases, a cogging torque value even as low as $\Delta\tau_{NL} \leq 0.5\%$ is mentioned, but for this paper, the given value is deemed sufficient in order to obtain a fair comparison between the different generator systems evaluated. With the efficiency of the slip-PMG unit given as $\eta_r = 97\%$ in [14] and to have an overall system efficiency of $\eta_t = \eta_s\eta_r \geq 91\%$, the efficiency of the PMSG should be no less than $\eta_s \geq 94\%$. It is also essential that the partial load efficiency be adequately evaluated as this is the region in which the wind generator will be operated most of the time. Furthermore, the short-circuit current level needs to be limited during low-voltage conditions to limit damage to the switch gear and transformers and also to protect the PMs from demagnetization.

IV. GENERATOR TOPOLOGIES CONSIDERED

For this paper, both nonoverlap single layer (SL) and double layer (DL) windings as shown in Fig. 2(a) and (b), respectively, are evaluated. Furthermore, in this paper, a new type of toroidal winding is also considered as shown in Fig. 2(c). Next to each machine structure, the slot layout with regard to the different phases is shown. For comparison, the phase layout of an SL

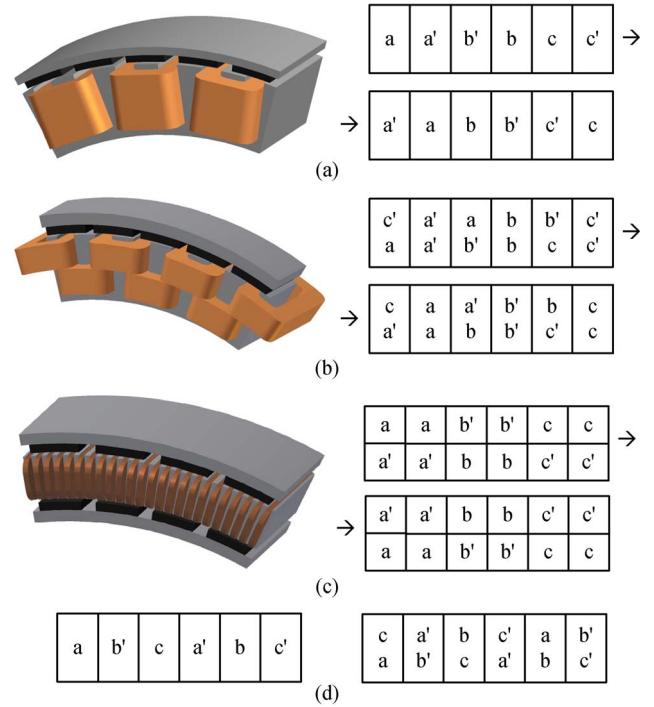


Fig. 2. (a) Nonoverlap SL and (b) DL. (c) Double-rotor toroidal 6 slot/pole PMSG winding structures and phase layouts and (d) conventional three-phase overlap winding SL and DL phase layouts.

and DL conventional three-phase overlap winding making use of three slots per pole is also shown in Fig. 2(d). The toroidally wound machine makes use of six slots per pole.

Nonoverlap winding PM machines have the advantages of easier manufacturing and segmentation as well as low cogging torque. In [25], a more elaborate discussion can be found on the torque characteristics of PM machines, with also further more relevant references on this aspect. The number of coils for the same pole number is also much lower, and preformed windings can easily be used by slightly adjusting the slot layout. This is even easier if an SL nonoverlap winding, where each alternating tooth is wound, is utilized and the amount of coils is also halved as opposed to the DL winding. However, the drawback of the SL nonoverlap winding as shown in previous studies is the large sub-MMF harmonic [25]. It is also known that the voltage quality of the SL winding is poorer than that of the DL winding. As for the design of the slip-PMG unit as in [14], the DL winding is also found to have a better performance than that of the SL nonoverlap winding machine. This is also shown in [27] regarding the design of direct-drive wind generators in general. As opposed to the DL winding configuration shown in Fig. 2(b), the coils can be placed adjacent to one another instead of stacked on top of one another. This will make the segmentation of the nonoverlap DL winding easier. Fig. 3(a) shows a FE field plot of the DL nonoverlap winding PM machine.

Overlap winding machines on the other hand are known to have a much better torque performance and should thus require less active and PM material for the same torque specifications as shown in [27]. These machines, however, have the problem of a very large torque ripple and a high number of coils. There are several well-known techniques available in the literature, such as skewing, to reduce the torque ripple of these machines. These

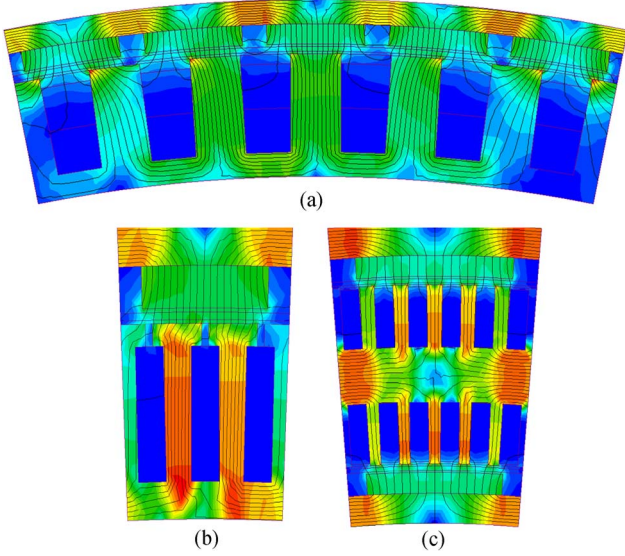


Fig. 3. FE field plots for the (a) nonoverlap DL, (b) conventional three phase overlap winding, and (c) double-rotor toroidal 6 slot/pole PMSGs.

methods, however, could increase the complexity and decrease the performance of the machine. In [25], a more complete discussion can be found on these different methods. On the other hand, the overlap winding machine makes use of a conventional three phase winding for which commercial winding processes have been available for a long time. A known problem for especially larger power levels, though, is the segmentation of the stator winding. The large end windings could also be a problem, particularly for machines with short axial lengths, typical of direct-drive wind generators. There are also questions regarding the effects that the known very low per-unit impedance of these machines will have, due to the direct-grid connection. In Fig. 3(b), an FE-simulated flux plot of a conventional overlap winding PM machine with three slots per pole is shown.

Dual rotor PM machine topologies have been proposed for both overlap and nonoverlap windings. However, in the case of overlap winding machines, the large end windings could make it difficult to assemble the machine, which means that the eventual configuration might not be at the optimum machine dimensions. In this case, it might be better to go for the toroidal type of topology such as in [28] and [29] and, more recently, as in [30] and [27] for direct drive wind generators. Normally toroidally wound coils are wound around a steel cylinder with the stator being toothless. This allows for easier manufacturing, but the drawback is a large air gap that requires more PM material. In this paper, a slotted stator configuration is used with slots on both the inner and outer diameters of the stator, as shown in Figs. 2(c) and 3(c) which shows the FE field plot of the toroidal winding machine. The machine is assembled in such a way that two opposing magnet polarities are facing one another. The flux from the bottom magnet thus links the bottom conductor, and the flux from the top magnet links the top conductor. Currently, it is difficult to comment on the manufacturability of the double rotor toroidal winding as this type of winding has not been extensively used before, particularly for large diameter wind turbines. However, segmentation for this type of winding should not be a problem due to none of the coils overlapping.

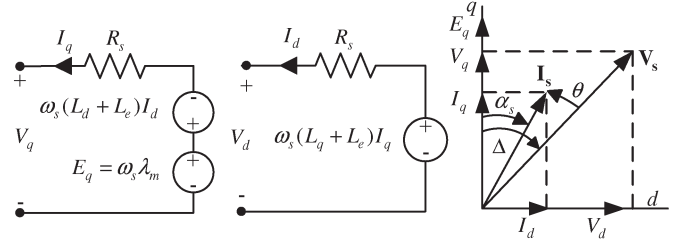


Fig. 4. dq -equivalent circuits and vector diagram for the modeling of the direct-grid PMSG.

Furthermore, as shown in [27], for the higher wind power categories (upper level of medium scale, and utility scale), the PM requirement and active mass of the nonoverlap winding topologies increase significantly as opposed to that of the overlap and toroidal winding topologies. This makes these winding types less favorable for higher wind power applications. For all the configurations in Fig. 3, negative boundary conditions are used in the FE analysis.

V. DESIGN METHODOLOGY

As mentioned in [4], it is not possible to know the operating state of the directly grid-connected PMSG as the current angle cannot be controlled as is the case for a PMSG connected to the grid via a solid-state converter. A special type of simulation procedure is thus required in conjunction with the design equations presented in this section. This procedure is thoroughly discussed in [4].

A. Design Equations

The directly grid-connected PMSG is modeled in the dq -reference frame fixed to the PM rotor. From the dq -equivalent circuits in Fig. 4, the steady-state dq -equivalent equations are given as

$$V_q = -R_s I_q - \omega_s (L_d + L_e) I_d + \omega_s \lambda_m \quad (1)$$

$$V_d = -R_s I_d + \omega_s (L_q + L_e) I_q. \quad (2)$$

V_d and V_q and I_d and I_q indicate the d - and q -axis voltages and currents, respectively. R_s is the per-phase resistance, and $\omega_s = 2\pi f_s$ indicates the synchronous electrical angular speed. The dq -inductances L_d and L_q are given as

$$L_q = \left| \frac{\lambda_q}{I_q} \right|; \quad L_d = \left| \frac{\lambda_d - \lambda_m}{I_d} \right|. \quad (3)$$

The end-winding inductance component is indicated by L_e , and the methods used to calculate this parameter are thoroughly discussed in [16]. It is found that end effects of both the windings and PMs can have a significant effect on the performance of the machine, particularly regarding the calculation of the maximum torque and current.

The general relations of voltage and current are given from Fig. 4 by

$$\begin{bmatrix} V_q \\ V_d \end{bmatrix} = \sqrt{2} V_{\text{rms}} \begin{bmatrix} \cos \Delta \\ \sin \Delta \end{bmatrix} \quad (4)$$

$$\begin{bmatrix} I_q \\ I_d \end{bmatrix} = \sqrt{2} I_{\text{rms}} \begin{bmatrix} \cos \alpha_s \\ \sin \alpha_s \end{bmatrix} \quad (5)$$

$$V_q^2 + V_d^2 = 2V_{\text{rms}}^2 \quad (6)$$

$$I_q^2 + I_d^2 = 2I_{\text{rms}}^2. \quad (7)$$

The per-phase grid voltage is fixed at $V_{\text{rms}} = 230$ V, and the stator current fed into the grid can be calculated as

$$I_{\text{rms}}^2 = \frac{P_{cu}}{3R_s} \quad (8)$$

with P_{cu} in (8) being the copper loss of the stator winding which is given as an input parameter. The developed torque is given by

$$T_s = \frac{3}{4}p[(L_q - L_d)I_d I_q + \lambda_m I_q] \quad (9)$$

and the efficiency is given by

$$\eta_s = \frac{T_s(2/p)\omega_s - (P_{cu} + P_{ecs} + P_{ecr} + P_{wf})}{T_s(2/p)\omega_s}. \quad (10)$$

The total generator losses are defined as $P_{cu} + P_{ecs} + P_{ecr} + P_{wf}$. P_{ecs} indicates the core losses in the stator steel. P_{ecr} includes the core losses in the rotor yoke as well as the PM eddy losses for the PM rotor. These values are calculated by means of FE analysis. The wind and friction losses are given by P_{wf} which is a fixed value for the fixed-speed SS-PMG system. Finally, the working power and reactive power supplying to or consuming from the grid are given as

$$\begin{bmatrix} P_s \\ Q_s \end{bmatrix} = 3V_{\text{rms}}I_{\text{rms}} \begin{bmatrix} \cos \theta \\ \sin \theta^* \end{bmatrix}. \quad (11)$$

The maximum breakdown torque that the generator is capable of when disconnected from the grid and braked by means of a connected brake-load resistance can be calculated as

$$T_b = \frac{3}{4}p\lambda_m^2 R_b \left[\frac{\omega_b^3(L_q - L_d)(L_q + L_e)}{(R_b^2 + \omega_b^2(L_d + L_e)(L_q + L_e))^2} \right] + \frac{3}{4}p\lambda_m^2 R_b \left[\frac{\omega_s}{(R_b^2 + \omega_b^2(L_d + L_e)(L_q + L_e))} \right] \quad (12)$$

with

$$\omega_b \approx \frac{R_b}{\sqrt{(L_d + L_e)(L_q + L_e)}} \quad (13)$$

as explained in [14] and [26]. R_b in (12) and (13) is the sum of R_s and the brake-load resistance used for braking [26].

B. Modeling Procedure

The aforementioned equations are used in the static modeling procedure coupled with an optimization algorithm as shown in Fig. 5 and thoroughly explained in [4]. The input parameters are indicated by \mathbf{X} , and the output parameters are indicated by \mathbf{Y} .

Initially, the current angle is assumed as $\alpha_s = 0$ with $I_d = 0$, and a first static FE iteration is solved. Initial values for the inductances can now be calculated with the assumption that $L_d \approx L_q$. With the inductance values known, an initial value for α_s can be calculated from (1)–(8). How the initial value for Δ is chosen is explained in [4]. With the current angle and peak current for each phase known, a second static FE iteration can be solved with L_d and L_q more accurately calculated in this case with (3). About three to four static FE iterations,

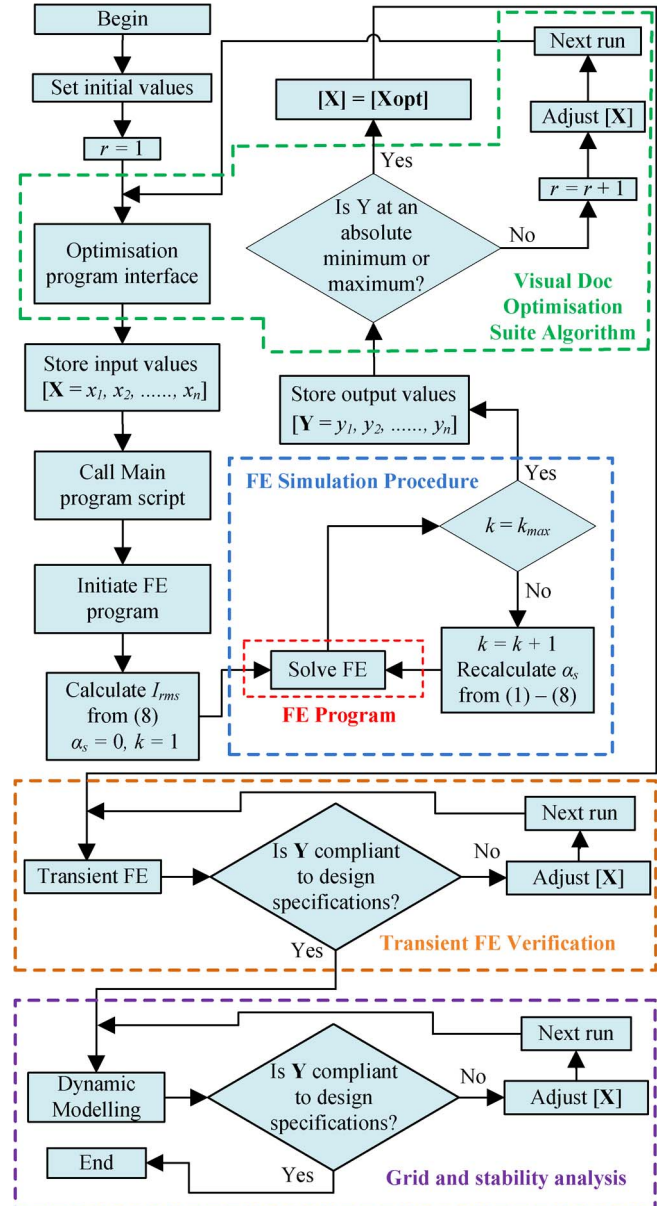


Fig. 5. Optimization program coupled with the simulation procedure and FE simulation program [4].

indicated by k in Fig. 5, are required to find the operating state of the generator at which the performance is simulated using the aforementioned equations. Static FE is much faster than transient FE, which means that optimization is much quicker.

After the initial static optimization, each optimum design is verified by means of transient FE, and slight adjustments are made to \mathbf{X} so that all the performance output parameters in \mathbf{Y} comply with the limits set in Section III. The reason for transient verification is to accurately calculate the torque ripple as well as the eddy current losses, which cannot be accurately calculated by static FE. Upon completion of the FE design iterations, a final check is done to determine if the generator design complies with the mentioned grid requirements. This is done with the help of the dynamic modeling methods as discussed in [15]. If the dynamic grid performance of the generator is not sufficient, the optimum FE design needs to be altered. The parameters which influence the grid behavior the most are

TABLE II
OPTIMIZATION RESULTS OF THE NONOVERLAP SL AND DL,
CONVENTIONAL THREE PHASE OVERLAP, AND DOUBLE
ROTOR TOROIDALLY WOUND PMSGs

	SL-non-overlap	DL-non-overlap	3 ϕ -overlap	Toroidal
T_{rated} , Nm	1000	1000	1000	1000
T_b , pu	2.22	2.16	3.11	4.40
$\Delta\tau_{NL}$, %	1.90	2.34	13.37	2.35
$\Delta\tau_L$, %	4.55	3.42	31.52	4.93
P_{ecs} , W	135.36	141.39	182.37	164.56
P_{ecr} , W	81.23	110.8	35.73	9.99
P_{cu} , W	604.18	588.48	683.78	711.71
η_s , W	94.57	94.44	94.01	94.00
D_o , mm	655	655	655	655
l , mm	129.0	125.0	114.5	80.00
D_i , mm	540.1	528.0	523.2	512.0
V_{rms} , V	230.0	230.0	230.0	230.0
I_{rms} , A	21.93	22.64	23.70	23.80
Δ , °	12.50	12.30	10.40	6.80
X_s , pu	0.247	0.208	0.082	0.068
PF	0.964	0.974	0.996	0.997
M_{PM} , kg	7.62	7.00	7.82	6.49
M_{Cu} , kg	16.69	20.16	25.22	21.04
M_{Fe} , kg	66.37	62.44	60.77	45.22
M_{Tot} , kg	90.68	89.61	93.91	71.43

SL non overlap: High active mass and PM content. Very easy manufacturing. Moderate to easy reduction of torque ripple. Low to moderate grid current harmonic content. Moderate to high short circuit current. Moderate response to grid voltage variations.

DL non overlap: High active mass and moderate PM content. Easy manufacturing. Easy reduction of torque ripple. Low to moderate grid current harmonic content. Moderate to high short circuit current. Moderate response to grid voltage variations.

3- ϕ overlap: High active mass and moderate PM content. Moderate to difficult manufacturing. Very high torque ripple. High grid current harmonic content. Extremely high short circuit current. Large unwanted reactive power flow if grid voltage varies from design value.

Double rotor toroidal: Low active mass and PM content. Moderate to difficult manufacturing. Moderate to easy reduction of torque ripple. High grid current harmonic content. Extremely high short circuit current. Large unwanted reactive power flow if grid voltage varies from design value.

typically the size of the synchronous reactance ($X_s = \omega_s L_s$) and the PM strength.

VI. OPTIMIZATION RESULTS

Table II gives the optimization results for the four PM machine topologies evaluated. An indication of the size of the machines can be found with l , the active length, and D_i , the inside diameter. The maximum outside diameter of all the machines is fixed at 655 mm. The active mass (M_{Tot}) of the four different generator topologies is minimized during optimization, subject to the design constraints discussed in Section III. The optimum PM mass (M_{PM}) for each machine topology is found with the help of Fig. 6. Shown in Fig. 6 are the active mass versus PM mass curves for each of the machine topologies. About three to four optimized points subject to a certain constraint for the PM mass are shown. Each optimum point needs to comply with the design constraints given in Section III. To calculate the minimum PM mass for each generator topology, the constraint for M_{PM} is reduced until the optimized structure no longer complies with the relevant specifications.

From Table II it is seen that the two nonoverlap winding machines and the conventional three phase overlap winding

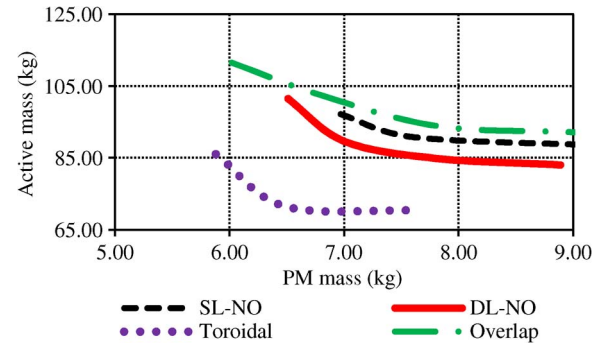


Fig. 6. Pareto front of active mass versus PM mass for the four PMSG machine topologies evaluated.

topology have more or less the same active mass, but with the optimum PM mass of the DL nonoverlap winding at a slightly lower value. The double rotor toroidal winding, on the other hand, has a significantly lower active mass and lower optimum PM mass than the rest of the generator topologies. The minimum value of M_{PM} for the conventional overlap winding and that of the double rotor toroidal winding are both lower than that of the rest of the machine structures. This is due to the much better torque performance of these machines, with the maximum breakdown torque of the overlap winding more than 3 p.u. and that for the double rotor toroidal winding more than 4 p.u. The rated torque of $1000 \text{ N} \cdot \text{m}$ is used as the base value. The reason for the much better performance regarding the active mass of the toroidal winding machine compared to the conventional overlap winding machine is due to the much shorter end windings of this winding configuration. In order to reduce the effect of the end windings, the active length is also much longer than that of the conventional overlap winding machine. Due to the nonoverlap winding machines having a much higher per-unit impedance, it is much more difficult for these machines to achieve the required maximum torque of $T_b > 2.0$ p.u. This is why the tendency of these machines during the design optimization is to increase the stator inner diameter in order to decrease the steel flux path, reducing the inductance of the machine. To achieve the required efficiency, the active length then needs to be increased.

Regarding the direct-grid connection of these different types of machines, there are also other aspects which need to be addressed such as those discussed previously in this paper. This relates to the PF of the machine, harmonic content of the current waveform, and the LVRT capabilities. The PF and reactive power consumption of all the topologies depend very much on the terminal voltage. It is evident that the overlap and toroidal winding machines operate at almost unity PF. Due to the lower value of the per-unit impedance X_s , this generator is more sensitive to grid voltage variations and also has a higher short-circuit current. For even small variations in the terminal voltage, large unwanted reactive power flow can occur. Both of these winding-type machines, particularly the conventional overlap winding machine, have a much higher harmonic content in the waveform of the current. Both these machines will thus need to be operated in conjunction with an additional series line reactance (SLR), which is not uncommon in power systems. The much better performance of the double-rotor toroidal winding

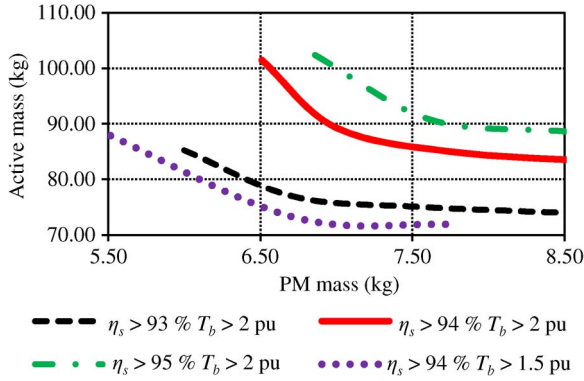


Fig. 7. Pareto front of active mass versus PM mass for four different design cases of the DL nonoverlap winding PMSG.

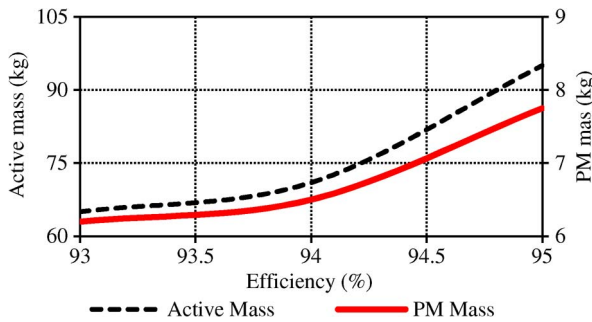


Fig. 8. Active and PM mass versus efficiency of the toroidally wound double-rotor PMSG.

needs to be weighed up against issues such as ease of manufacturing and the suitability of this generator for direct-grid connection.

The results shown in Fig. 7 for different efficiencies and maximum torque specification of the DL nonoverlap winding machine are very interesting. When increasing the minimum efficiency from 94% to 95%, no major increase in mass is observed. However, when decreasing the maximum torque requirement from $T_b > 2.0$ p.u. to $T_b > 1.5$ p.u., a significant reduction in mass is seen. This also explains the slightly higher efficiencies of the nonoverlap winding machines in Table II as the maximum torque requirement for the nonoverlap winding machines is a much more difficult parameter to comply with than the specified minimum efficiency. The relationship between active mass and PM content versus efficiency is shown for the double-rotor toroidally wound machine in Fig. 8. Only a marginal increase in active mass and PM content is observed when changing the minimum efficiency specification from $\eta_s > 93\%$ to $\eta_s > 94\%$. However, for $\eta_s > 95\%$, a significant increase in active mass and PM content is observed.

VII. PROTOTYPE MACHINE EVALUATION

Two SS-PMGs were manufactured and practically evaluated. SS-PMG 1 makes use of a nonoverlap SL winding PMSG and a nonoverlap DL winding slip-PMG. SS-PMG 2 makes use of a nonoverlap DL winding PMSG and a conventional overlap cage winding slip-PMG. Fig. 9 shows SS-PMG 2 mounted on the test bench. Fig. 10 show SS-PMG 1 and SS-PMG 2 installed and being tested in the field.



Fig. 9. Prototype 15-kW SS-PMG 2 on the test bench, connected to a driving motor on the right, through a torque sensor shown in the middle.



Fig. 10. SS-PMGs 1 and 2 integrated as complete wind turbine systems, being field tested.

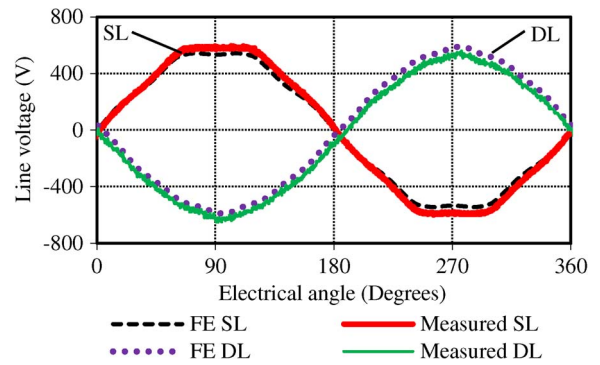


Fig. 11. Open-circuit line voltages versus electrical angle of SS-PMG 1 and SS-PMG 2.

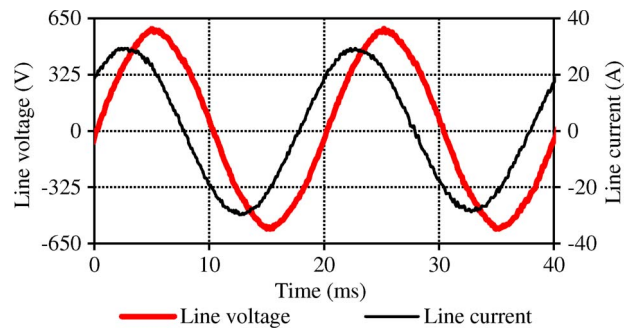


Fig. 12. Measured grid voltage and line current of SS-PMG 2 during field testing.

Fig. 11 shows the open-circuit FE-simulated and measured line voltages of SS-PMGs 1 and 2. The nonoverlap DL winding has a much more sinusoidal voltage waveform as opposed to the SL winding. Fig. 12 shows the measured grid line voltage and current being fed to the grid by SS-PMG 2 during field testing

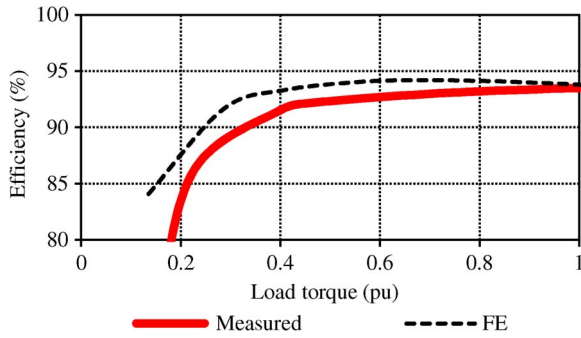


Fig. 13. FE predicted and measured efficiency versus load torque of SS-PMG 2.

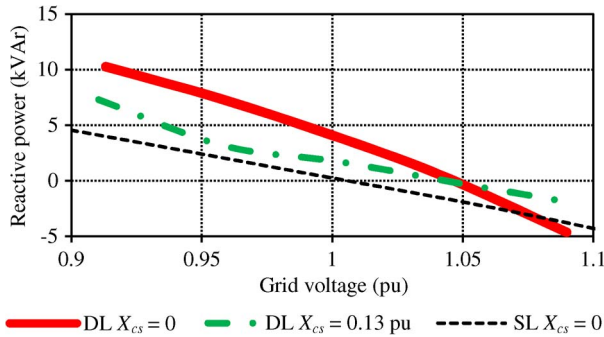


Fig. 14. Measured reactive power versus per-unit grid voltage at zero load of SS-PMG 1 and SS-PMG 2 with and without an SLR.

at the rated wind speed of $v_w = 11$ m/s. The measured and FE-simulated efficiency versus load torque of SS-PMG 2 is shown in Fig. 13.

The measured reactive power flow versus terminal voltage at zero load of SS-PMG 1 and SS-PMG-2 with and without an SLR (X_{cs}) is shown in Fig. 14. This is typically what will happen during low-voltage conditions, when the generator will help support the grid voltage. Furthermore, it is clear that, with a higher series reactance, the generator is much less susceptible to unwanted reactive power flow due to grid voltage variations. Positive reactive power indicates reactive power being delivered to the grid, and negative values indicate the absorption of reactive power.

Fig. 15 shows the PF versus load of SS-PMGs 1 and 2 for variations in terminal voltage and for different combinations of series (X_{cs}) and parallel compensation (C_p and L_p). As specified by the relevant grid code for small-scale systems, the generator needs to continuously operate in a +10% and -15% band of the rated grid voltage. Grid compliance regarding PF could be realized by switching in passive circuit elements as shown in Fig. 15, making use of the tap-changing transformer scheme of [20], or by utilizing a static VAR compensator (SVC). Although the SVC introduces active power switches to the system, it is only partially rated. Also, as seen in Fig. 15, it will only mostly be required in the partially rated region and will only be active when grid voltage variations occur.

Fig. 16 shows the THD of SS-PMG 2 versus generator load. As stated in Section III, the THD should be below 5%. It is seen that, by increasing X_{cs} , grid compliance can be achieved in this regard. The series impedance acts as a buffer between the

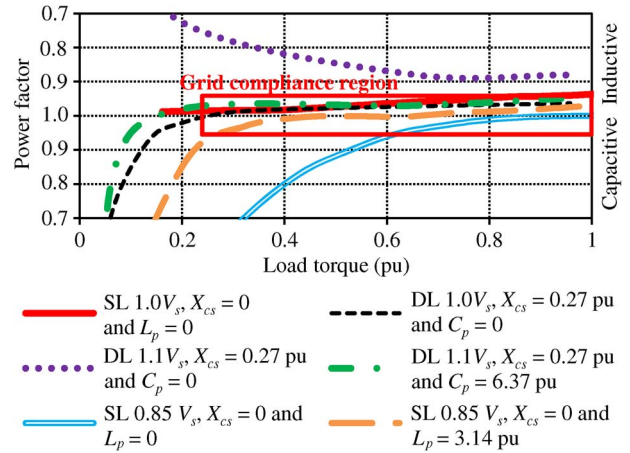


Fig. 15. Measured PF versus per-unit load power of SS-PMGs 1 and 2 for variations in grid voltage and different combinations of passive compensation elements.

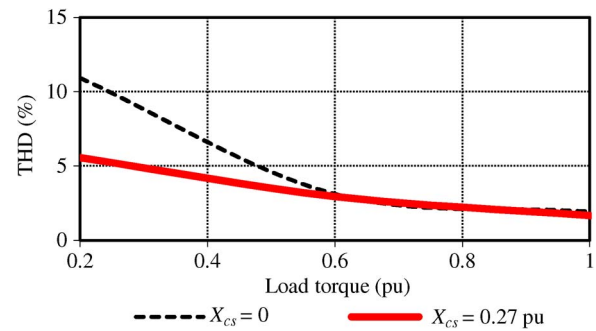


Fig. 16. THD versus load torque for $X_{cs} = 0$ and $X_{cs} = 0.27$ p.u. for SS-PMG 2.

generator and grid to limit the flow of harmonic currents. As there are different limit sets for the different harmonics, these should be individually evaluated in order to make sure that the generator complies to the relevant specifications.

VIII. CONCLUSION

It is clearly shown in this paper that a different design approach needs to be followed for directly grid-connected PMSGs as opposed to conventional PM generator configurations connected to the grid via a power electronic converter. The generator design needs to comply with all the requirements stipulated in the relevant grid codes. In this paper, a design approach is devised where the generator is optimized by means of a static FE modeling method coupled with an optimization algorithm. The design is verified by means of transient FE analysis and a dynamic modeling procedure to determine whether the design is stable and if it is suitable for direct-grid connection. Even though the focus in this paper is on the design of wind generators, the same design approach is valid for all applications where PM machines are connected directly to the grid. The relevant grid connection requirements will be determined by the application.

In this case, the proposed toroidally wound double rotor PMSG is shown to give the best performance regarding active mass and PM content. The manufacturing of this generator is, however, still a question as it is an unknown concept in

direct-drive wind generator design. Furthermore, aspects such as power quality and the low synchronous reactance make this generator less suitable for direct-grid connection. The nonoverlap SL winding machine is the easiest to manufacture and has the highest value of X_s but has the highest active mass, and the current waveform also has a higher harmonic content than that of the DL nonoverlap winding. From this paper, it seems that, for the investigated 15-kW power level, the DL nonoverlap winding machine is the most favorable topology regarding mass, power quality, direct-grid connection, and manufacturability. However, it is important to note that, for higher power levels, the difference in mass and PM content between the nonoverlap winding machines and the overlap winding and toroidally wound machines will increase. Furthermore, it is also shown how additional compensation devices of low complexity can be used in the system to help it comply with the grid-code specifications.

REFERENCES

- [1] H. Polinder *et al.*, "Trends in wind turbine generator systems," *IEEE J. Emerging Sel. Topics Power Electron.*, vol. 1, no. 3, pp. 174–185, Sep. 2013.
- [2] M. Arifujjaman, M. T. Iqbal, and J. E. Quicoe, "Reliability analysis of grid connected small wind turbine power electronics," *Appl. Energy*, vol. 86, no. 9, pp. 1617–1623, Sep. 2009.
- [3] M. Wilkinson *et al.*, "Methodology and results of the Reliawind reliability field study," in *Proc. EWEC*, Warsaw, Poland, 2010, pp. 1–7.
- [4] J. H. J. Potgieter and M. J. Kamper, "Design of new concept gearless direct-grid connected slip-synchronous permanent magnet wind generator," *IEEE Trans. Ind. Appl.*, vol. 48, no. 3, pp. 913–922, May/June 2012.
- [5] A. J. G. Westlake, J. R. Bumby, and E. Spooner, "Damping the power-angle oscillations of a permanent-magnet synchronous generator with particular reference to wind turbine applications," in *Proc. Inst. Elect. Eng.—Electr. Power Appl.*, 1996, vol. 143, no. 3, pp. 269–280.
- [6] S. Grabic, N. Celanovic, and V. A. Katic, "Permanent magnet synchronous generator cascade for wind turbine application," *IEEE Trans. Power Electron.*, vol. 23, no. 3, pp. 1136–1142, May 2008.
- [7] H. Müller, M. Pöller, A. Basteck, M. Tilshcher, and J. Pfister, "Grid compatibility of variable speed wind turbines with directly coupled synchronous generator and hydro-dynamically controlled gearbox," in *Proc. 6th Int. Workshop Largescale Integr. Wind Power Transmiss. Netw. Off-shore Wind Farms*, Delft, The Netherlands, 2006, pp. 307–313.
- [8] S. H. Salter and M. Rea, "Hydraulics for wind," in *Proc. EWEC*, Hamburg, Germany, 1985, pp. 1–8.
- [9] A. Izadian, S. Hamzehlouia, M. Deldar, and S. Anwar, "A hydraulic wind power transfer system: Operation and modeling," *IEEE Trans. Sustain. Energy*, vol. 5, no. 2, pp. 457–465, Apr. 2014.
- [10] F. Punga and L. Schon, "Der neue kollektorlose Einphasenmotor der Firma Krupp," *Elektrotech. Zeitschrift*, vol. 47, no. 29, pp. 877–881, 1926.
- [11] B. Hagenkort, T. Hartkopf, A. Binder, and S. Jöckel, "Modelling a direct drive permanent magnet induction machine," in *Proc. ICEM*, Espoo, Finland, 2000, pp. 1495–1499.
- [12] E. Troster, M. Sperling, and T. Hartkopf, "Finite element analysis of a permanent magnet induction machine," in *Proc. Int. SPEEDAM*, Taormina, Italy, 2006, pp. 179–184.
- [13] A. Thomas, "A doubly-fed permanent magnet generator for wind turbines," M. S. thesis, Massachusetts Inst. Technol., Cambridge, MA, USA, 2004.
- [14] J. H. J. Potgieter and M. J. Kamper, "Optimum design and comparison of slip permanent-magnet couplings with wind energy as case study application," *IEEE Trans. Ind. Appl.*, vol. 50, no. 5, pp. 3223–3234, Sep./Oct. 2014.
- [15] J. H. J. Potgieter and M. J. Kamper, "Modelling and stability analysis of a direct-drive-direct grid slip-synchronous permanent magnet wind generator," *IEEE Trans. Ind. Appl.*, vol. 50, no. 3, pp. 1738–1747, May/June 2014.
- [16] J. H. J. Potgieter and M. J. Kamper, "Calculation methods and effects of end-winding inductance and permanent-magnet end flux on performance prediction of nonoverlap winding permanent-magnet machines," *IEEE Trans. Ind. Appl.*, vol. 50, no. 4, pp. 2458–2466, Jul./Aug. 2014.
- [17] E. Muljadi, V. Gevorgian, M. Singh, and S. Santoso, "Understanding inertial and frequency response of wind power plants," in *Proc. IEEE Symp. Power Electron. Mach. Wind Appl.*, Denver, CO, USA, 2012, pp. 1–8.
- [18] "Grid connection code for renewable power plants (RPPs) connected to the electricity transmission system (TS) or the distribution system (DS) in South Africa," Germiston, South Africa, Nov. 2012, Version 2.6.
- [19] U. Hoffmann, P. Bouwer, and M. J. Kamper, "Direct grid connection of a slip-permanent magnet wind turbine generator," in *Proc. IEEE ECCE*, Phoenix, AZ, USA, 2011, pp. 2373–2380.
- [20] A. T. Spies and M. J. Kamper, "Reactive power control of a direct grid connected slip synchronous permanent magnet wind generator," in *Proc. IEEE ICIT*, Cape Town, South Africa, 2013, pp. 770–775.
- [21] U. Hoffmann and M. J. Kamper, "Low voltage ride-through compensation for a slip-permanent magnet wind turbine generator," in *Proc. SAUPEC*, Cape Town, South Africa, 2011, pp. 191–196.
- [22] "GRID interconnection of embedded generation Part 2: Small-scale embedded generation," Sunninghill, South Africa, NRS 097-2-1, 2010, Technology Standardization Department (TSD).
- [23] H. Polinder, F. F. A. van der Pijl, G. J. de Vilder, and P. Tavner, "Comparison of direct-drive and geared generator concepts for wind turbines," *IEEE Trans. Energy Convers.*, vol. 21, no. 3, pp. 725–733, Sep. 2006.
- [24] R. Scott Semken *et al.*, "Direct-drive permanent magnet generators for high power wind turbines: Benefits and limiting factors," *IET Renew. Power Gen.*, vol. 6, no. 1, pp. 1–8, Jan. 2012.
- [25] J. H. J. Potgieter and M. J. Kamper, "Torque and voltage quality in design optimisation of low cost non-overlap single layer winding permanent magnet wind generator," *IEEE Trans. Ind. Electron.*, vol. 59, no. 5, pp. 2147–2156, May 2012.
- [26] J. H. J. Potgieter and M. J. Kamper, "Design considerations in the implementation of an electromagnetic brake for a 15 kW PM wind generator," in *Proc. SAUPEC*, Potchefstroom, South Africa, 2013, pp. 98–103.
- [27] J. H. J. Potgieter and M. J. Kamper, "Evaluation, application and comparison of a double-rotor toothed toroidal winding wind generator over a wide power range," in *Proc. ICEM*, Berlin, Germany, 2014, pp. 1158–1164.
- [28] R. Qu and T. Lipo, "Dual-rotor, radial-flux, toroidally wound permanent-magnet machines," *IEEE Trans. Ind. Appl.*, vol. 39, no. 6, pp. 1665–1673, Nov./Dec. 2003.
- [29] Y. Yeh, M. Hsieh, and D. Dorell, "Different arrangements for dual-rotor dual-output radial-flux motors," *IEEE Trans. Ind. Appl.*, vol. 48, no. 2, pp. 612–622, Mar./Apr. 2012.
- [30] P. Xu, X. Liu, K. Shi, and Y. Du, "Design of dual-rotor radial flux permanent-magnet generator for wind power applications," *Appl. Mech. Mater.*, vol. 416/417, pp. 9–14, 2013.



Johannes H. J. Potgieter (M'15) received the B.Eng. degree in electrical and electronic engineering and the M.Sc. (Eng.) and Ph.D. (Eng.) degrees in electrical engineering from the University of Stellenbosch, Stellenbosch, South Africa, in 2008, 2011, and 2014, respectively.

Since May 2014, he has been a Postdoctoral Research Assistant at the University of Oxford, Oxford, U.K. His research interests include wind power generation technologies, hybrid-electrical automotive drivetrain solutions, and the design and optimization of permanent-magnet and switched reluctance electrical machines.



Maarten J. Kamper (SM'08) received the M.Sc. (Eng.) and Ph.D. (Eng.) degrees from the University of Stellenbosch, Stellenbosch, South Africa, in 1987 and 1996, respectively.

He has been with the academic staff of the Department of Electrical and Electronic Engineering, University of Stellenbosch, since 1989, where he is currently a Professor of electrical machines and drives. His research interests include computer-aided design and control of reluctance, permanent-magnet, and induction machine drives.

Prof. Kamper is a South African National Research Foundation Supported Scientist and a Registered Professional Engineer in South Africa.